Angle-Dependent Light Scattering Study of Silica Aggregate Growth in 1-D Methane/Air Flames with Hexamethyldisiloxane Admixture

Langenkamp, Peter N.; Mokhov, Anatoli V.; Levinsky, Howard B.

Published in:
Combustion Science and Technology

DOI:
10.1080/00102202.2016.1193500

Publication date:
2017

Taylor & Francis
Taylor & Francis Group

Combustion Science and Technology

ISSN: 0010-2202 (Print) 1563-521X (Online) Journal homepage: http://www.tandfonline.com/loi/gcst20

Angle-Dependent Light Scattering Study of Silica Aggregate Growth in 1-D Methane/Air Flames with Hexamethyldisiloxane Admixture: Effects of Siloxane Concentration, Flame Temperature, and Equivalence Ratio

Peter N. Langenkamp, Anatoli V. Mokhov & Howard B. Levinsky

To cite this article: Peter N. Langenkamp, Anatoli V. Mokhov & Howard B. Levinsky (2017) Angle-Dependent Light Scattering Study of Silica Aggregate Growth in 1-D Methane/Air Flames with Hexamethyldisiloxane Admixture: Effects of Siloxane Concentration, Flame Temperature, and Equivalence Ratio, Combustion Science and Technology, 189:1, 132-149, DOI: 10.1080/00102202.2016.1193500

To link to this article: https://doi.org/10.1080/00102202.2016.1193500

Accepted author version posted online: 07 Jun 2016.
Published online: 07 Jun 2016.

COMBUSTION SCIENCE AND TECHNOLOGY
2017, VOL. 189, NO. 1, 132–149
http://dx.doi.org/10.1080/00102202.2016.1193500

Taylor & Francis
Taylor & Francis Group

Angle-Dependent Light Scattering Study of Silica Aggregate Growth in 1-D Methane/Air Flames with Hexamethyldisiloxane Admixture: Effects of Siloxane Concentration, Flame Temperature, and Equivalence Ratio

Peter N. Langenkamp[a], Anatoli V. Mokhov[a], and Howard B. Levinsky[a,b]

[a]University of Groningen, Faculty of Mathematics and Natural Sciences, Energy and Sustainability Research Institute Groningen, Laboratory of Higher Temperature Energy Conversion, Groningen, the Netherlands; [b]DNV GL, Oil & Gas, Groningen, the Netherlands

ABSTRACT

Silica aggregate formation was studied in 1D premixed methane/hexamethyldisiloxane/air flames by angle-dependent light scattering measurements for various siloxane concentrations, flame temperatures, and equivalence ratios, using Guinier analysis to interpret the experimental data. A sublinear dependence of the aggregate radii of gyration R_g of generated silica particles on residence time, and non-monotonic dependence on flame temperature with a maximum around 2000 K have been observed, with radii of gyration R_g in the range of 10 to 120 nm. Furthermore, a lean flame environment appears to foster aggregate growth compared to rich and stoichiometric flames, in which growth is very similar. When fixing the initial conditions at the residence time corresponding to the first measurement point, a simple model describing particle evolution as a result of collisional growth and sintering predicts well the functional dependence of the growth of particle radii.

ARTICLE HISTORY
Received 2 February 2016
Revised 14 March 2016
Accepted 20 May 2016

KEYWORDS
Aggregates; Combustion; Diagnostics; Kinetics; Silica

Introduction

Concerns over the climate, dwindling energy reserves, and the desire for energetic independence are driving the development of renewable energy sources. Biogases can play an important role in a transition from fossil fuels and have seen increasing utilization in recent years; growth in biogas production and use is expected to continue for the foreseeable future (van Foreest, 2012). While the exact composition depends on the source, biogas is typically composed of methane and carbon dioxide, with trace amounts of other constituents, such as sulfide compounds, aromatic and halogenated compounds, and volatile compounds such as siloxanes (Rasi, 2009).

As an impurity in biofuels, siloxanes are of particular interest. Silicon dioxide generated in the combustion of the siloxanes coalesces into particles that subsequently form aggregates and deposit on internal parts of combustion equipment. This can eventually lead to damage and even equipment failure, which puts limits on acceptable siloxane concentrations (Turkin et al., 2014). Whereas the size and structure of silica particles determine their

CONTACT Anatoli V. Mokhov a.v.mokhov@rug.nl University of Groningen, Faculty of Mathematics and Natural Sciences, Energy and Sustainability Research Institute Groningen, Laboratory of High Temperature Energy Conversion, Nijenborgh 4, Groningen, 9747 AG Netherlands.

Color versions of one or more of the figures in the article can be found online at www.tandfonline.com/gcst.

mechanical properties as ceramic powders (Pratsinis, 1998), the structure of silica aggregates are also critical determinants for the impact of deposition in combustion equipment. The deposition of 'fluffy' fractal structures will result in more blocked volume in a heat exchanger than a denser layer for the same mass of deposited silica; changes in equipment performance have been attributed to this effect (Gersen et al., 2013). Therefore, a model describing the growth and properties of these aggregates reliably is essential for formulating realistic limits.

An analytic approach for describing particle growth (Smirnov, 2011) can be very instructive, as it provides insight into functional dependencies, but is of limited quantitative value because of the system's complexity. Similarly, numerical models (Lee et al., 2001a, 2001b; Shekar et al., 2012; Suh et al., 2001; Xiong et al., 1993; Zachariah and Semerjian, 1989) are as yet unreliable because the kinetics of silica aggregate formation are not well known. Therefore, experimental studies to characterize the aggregates are indispensable to gain a better understanding of processes of silica formation in combustion environments.

Previous studies of silica formation in flames have been motivated by synthesis of ceramic powders (Pratsinis, 1998). In these studies, particle generation has been investigated mainly in diffusion flames at atmospheric pressure (Bae and Shin, 2009; Choi et al., 1999; Jang, 1999; Rulison et al., 2011; Suh et al., 2006; Wooldridge et al., 2002; Zachariah et al., 1989a; Zhu and Pratsinis, 1997). Because of the spatially varying temperature and local fuel/oxidizer ratios in these systems, the results of these studies are difficult to interpret unambiguously, particularly regarding processes that occur at relatively short time scales. Furthermore, many of these studies used silane (SiH_4) as the source of silicon. Given the pyrophoric nature of this compound, complete premixing of the silicon source with the fuel-air mixture is problematical and the introduction of SiH_4 occurred diffusively (see, for example, Wooldridge (1998) and references therein). This gives rise to uncertainties in the actual local concentrations of silica precursors. The use of siloxanes, which are relatively stable in air, opened the door to premixed studies with well-defined local concentrations, as summarized in Jalali et al. (2013). One-dimensional (1D) premixed flames yield conditions more amenable to analysis and, as discussed below, can be varied in a straightforward manner. Using ex-situ particle sampling, Smirnov et al. (2012), for example, analyzed aggregate growth and primary particle size as function of residence time in this type of flame based on transmission electron microscopy (TEM). Other studies in premixed 1D flames employed in-situ techniques, such as dynamic light scattering (Flower and Hurd, 1987; Hurd and Flower, 1988) and angle dependent light scattering (ADLS) (Chang et al., 1998; Ulrich and Riehl, 1982), to characterize silica growth as function of time. In-situ measurements have a clear advantage over ex-situ methods, such as TEM, in that they obviate the need for intrusive physical sampling. In addition to being more time efficient, in-situ measurement removes the uncertainties related to disturbing the particle growth processes in the flame as a result of sampling.

Previous in-situ studies in 1D premixed flames also varied a limited number of experimental parameters. For example, Ulrich and Riehl (1982) examined different silica concentrations in the fuel/oxidizer mixture and altered the temperatures in a turbulent jet flame by varying the equivalence ratio. They also performed experiments on flames stabilized on a honeycomb flame holder, but the reduction in flame temperature was not characterized. Chang et al. (1998) investigated the effect of adding $POCl_3$ vapor to depress the melting point of silica on silica agglomerate morphology. To our knowledge, no studies have been done that systematically vary flame temperature independently from

the equivalence ratio, which is readily obtained in 1D premixed flames (Sepman et al., 2011). Furthermore, given the interest of the prior studies in the synthesis of ceramic powders, the range of concentrations in studies that examined the effects of precursor concentration (Jalali et al., 2013) are generally above 0.15 mol%. In this article we present results obtained using ADLS to study silica aggregate growth in 1D premixed flames using hexamethyldisiloxane $C_6H_{18}Si_2O$ (abbreviated as L2) as silica precursor. Here, we investigate aggregate growth as a function of residence time for a wide range of experimental conditions, varying silica concentration, flame temperature, and equivalence ratio. We emphasize here that the flame conditions considered in this study are those that actually occur in combustion equipment; in fact, the burner configuration used, the residence times covered, and the variations examined (Mokhov and Levinsky, 2000) are nearly identical to those in millions of appliances used for domestic heating. As such, this study contributes towards identifying the conditions germane for silica deposition when burning siloxane-containing biogases.

Experimental procedure

Burner system and gas supply

Silica aggregates are produced in flat, premixed methane/L2/air flames at atmospheric pressure using the system shown schematically in Figure 1. The flames are stabilized above a perforated ceramic burner deck with a diameter of 60 mm, as used previously (Mokhov and Levinsky, 2000). A tubular chimney with a diameter of 80 mm is placed downstream to suppress flow instabilities. The axial distance between the measuring volume and the burner surface (HAB) is varied by moving the burner by a positioner (Parker) axially in 5-mm steps.

Flames of various temperatures and fuel equivalence ratios are obtained by setting appropriate air and methane mass fluxes using Alicat MC-series mass flow controllers with a specified accuracy of ±1% full scale. The flow rates in this study were always higher than 10% of full scale of the flow controllers used for their measurement. Additionally, the flow rates were measured by Bronkhorst mass flow meters. Differences between the measured and set values of flows were less than 2%, in the working range from 10 to 40 SLPM (298 K, 1 atm). The flame temperature is varied by changing the mass flux through the burner while keeping the fuel/air ratio constant (Mokhov and Levinsky, 2000; Sepman et al., 2011). Three equivalence ratios, φ, are studied here, φ = 0.8, 1, and 1.3. Since prior

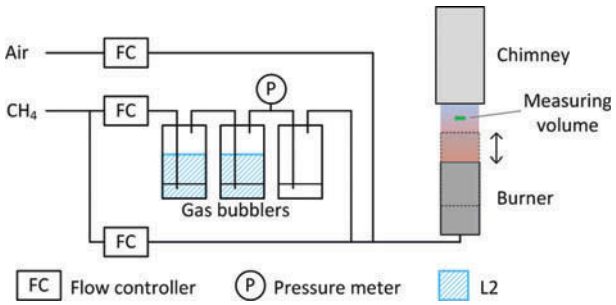

Figure 1. Burner system and gas supply.

studies (Mokhov and Levinsky, 2000; Sepman et al., 2011, 2013) showed that the measured maximum temperatures and those determined by solving the 1D governing equations for burner-stabilized flames agree to within 50 K, here we compute the flame temperature. The results obtained by using the code from the Cantera suite (Goodwin et al., 2015) with the GRI-Mech 3.0 chemical mechanism (Smith et al., n.d.) are shown in Figure 2. In the figure, the mass flux is recast as a linear exit velocity of the 1D fuel-air mixture, anticipating the conversion to residence times below. Experiments under similar conditions (Mokhov et al., 2013) indicate that, for the region of measurement examined here (see below), the temperatures were generally constant up to ~30 mm, followed by a slow decrease. At the lowest mass fluxes described below, axial distance of constant temperature is less than 20 mm. Since the siloxane fractions studied are relatively low, we neglect any contribution of the presence of siloxanes on the computed temperatures.

L2 was added to the unburned methane/air mixture by passing a fraction of the methane flow through a bubbler system containing liquid L2 with a purity of >98.5% (Sigma-Aldrich 52630 FLUKA). The mole fraction of L2 in the unburned gas mixture can be calculated from the relative volume flows and pressure as:

$$X_{L2} = \left(\frac{P_{L2}}{P_{Bub}}\right)\left(\frac{Q_{Bub}}{Q_{Total}}\right)$$

where P_{L2} is the (temperature dependent) vapor pressure of L2, P_{Bub} is the pressure in the bubbler system, and Q_{Bub} and Q_{Total} are the standard volumetric flow through the bubblers and of the gas mixture through the burner, respectively. Weighing the siloxane cylinder before and after a few hours of operation has shown that P_{L2} is close to that of saturated vapor (5.59 kPa at 298 K; Flaningam, 1986). All measurements were performed at the same temperature (298 K) and pressure (295 kPa) inside the bubblers. Mole fractions of L2 in the total methane/air mixture ranging from 150 to 800 ppm were obtained by varying the fraction of methane passing through the bubbler system, with an estimated day-to-day reproducibility of better than 10%. Since oxidation of one L2 molecule

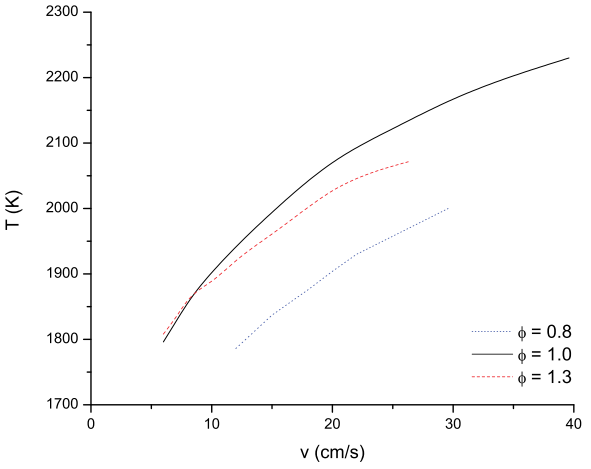

Figure 2. Flame temperature as a function of exit velocity for lean, stoichiometric, and fuel-rich flames, obtained from solving governing equations describing 1-D burner-stabilized flames.

produces two SiO_2 molecules, while the number of moles in the gas mixture does not change significantly during combustion, we consider $X_{SiO_2} = 2X_{L2}$. Below, we will only refer to the concentration of Si in the combustion products.

Optical setup

A schematic of the optical measuring system used for the ADLS measurements is shown in Figure 3. The laser beam from a 532-nm cw laser (Coherent Sapphire) with a power of 100 mW is focused above the center of the burner at 20 mm below the chimney by a lens with a focal length of 500 mm producing a focal spot with a diameter less than 1 mm. The scattered light is collected by $f/4$, 100 mm focal length lenses in the horizontal scattering plane at four different angles (42°, 62°, 90°, and 133°) with respect to the forward direction of the laser beam. Each lens is placed at 20 cm from the center of the burner producing a 1:1 image of the laser beam onto a detector. Because detection occurs at the laser's wavelength, great care has to be taken to avoid detection of light not coming from the intended detection volume as it could overwhelm the signal we want to detect. Ambient light is suppressed by narrow band filters centered at 532 nm with a bandwidth of 3 nm (Thorlabs FL532-3) placed in front of the detector. A linear polarizer (Thorlabs LPVISE100-A) is included as well, to reject horizontally polarized light. Also, to prevent detecting scattered light from other parts of the experimental setup the collecting optics are assembled in a tube system.

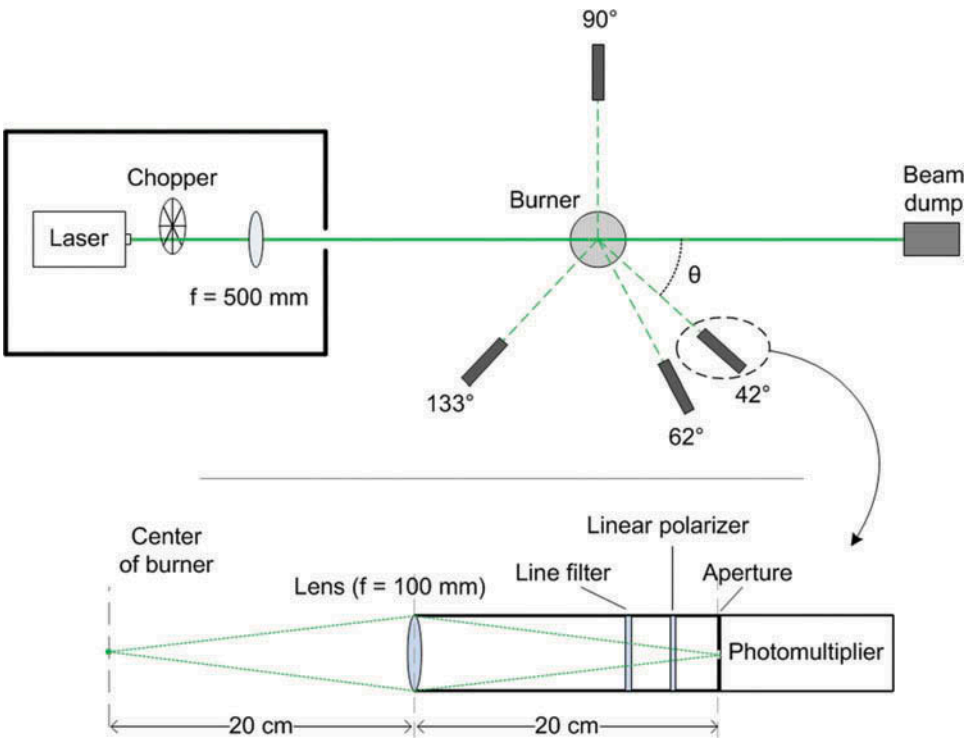

Figure 3. Schematic for the ADLS experimental setup. The angular orientations of the collection systems are with respect to the forward direction of the laser beam.

Rectangular apertures are placed directly in front of the detectors to set the measuring volume. The length of the measuring volume in the direction along the laser beam l_s is determined by the aperture's width d and the scattering angle θ, $l_s = d/\sin(\theta)$. The apertures' widths are tailored to each collection system's angular position, such that all detectors collect the light from the same 7.5-mm section of the laser beam, which is less than a third of the region where the temperature profile is uniform according to measurements performed in similar flames (Mokhov et al., 2013) in the same burner geometry. The apertures' height (1.5 mm) exceeds the laser beam diameter to avoid the effect of possible beam steering. Photomultipliers (Hamamatsu H10721-210) are used as detectors. To increase the signal-to-noise ratio, the laser beam is modulated at 650 Hz using a chopper wheel and the signal is measured by a lock-in amplifier (EG&G Instruments 7265 DSP). The chopper is contained in an enclosure along with the laser and focusing lens to reduce the stray light entering the collection systems. The photomultipliers were operated at an applied voltage of 800 V, providing signals in the range 0.5–100 mV at input resistance 25 kΩ with acceptable signal-to-noise ratio. The linearity of the detection system has been verified by varying laser intensity with an attenuator and measuring laser power with a calibrated photodiode.

The signals measured by the photomultipliers are recorded simultaneously, and normalized to take into account variations in transmittances and sensitivities between the individual collection systems (which result in signal differences of up to 30%). The normalization coefficients are determined by measuring the intensity of Rayleigh scattering in sulfur hexafluoride (SF_6), purged through the burner. Due to its high cross section (Sneep and Ubachs, 2005), Rayleigh scattering from this gas provides a strong isotropic signal that minimizes the relative contribution of any detected background light. The background contribution to the measured signal is determined by measuring the ratio of scattered signals in SF_6 (I_{SF_6}) and air (I_{air}) using the formula:

$$\frac{I_{SF_6}}{I_{air,}} = \frac{\frac{\sigma_{SF_6}}{\sigma_{air}} + \alpha_{bg}}{1 + \alpha_{bg}} \tag{1}$$

where the ratio of the Rayleigh cross sections of SF_6 and air, $\sigma_{SF_6}/\sigma_{air}$, is approximately 6.3 (Sneep and Ubachs, 2005), and α_{bg} is the background signal normalized by the intensity of Rayleigh scattering in air. In this work α_{bg} was always less than 2.5%, while the signal in flames with particles typically exceeds the signal in air by more than one order of magnitude, eliminating the necessity for background correction when processing measured signals.

Data processing

The measured signal produced by scattered light from identical aggregates containing n spherical particles (monomers) of radius r_m is given by (Sorensen, 2001):

$$I(q) = c_0 I_0 N_p n^2 k^4 r_m^6 FS \tag{2}$$

where c_0 is a constant accounting for parameters of the optical setup, such as sampling volume, collecting angle, etc.; I_0 is the incident intensity; N_p is the concentration of aggregates; F is a function of the refractive index of a monomer; and $k = 2\pi/\lambda$ is the magnitude of the scattered wave vector $\vec{k}$ at exciting laser wavelength λ. The so-called

structure factor S in Eq. (2) arises from the interference of scattered waves produced by aggregates' monomers:

$$S = n^{-2}\left|\sum_{n}^{i} e^{i\vec{q}\cdot\overrightarrow{r_i}}\right|^2 \tag{3}$$

where $\vec{q} = 2\vec{k}\sin(\theta/2)$ is the scattering wave-vector at scattering angle θ and $\overrightarrow{r_i}$ is the position of a monomer in the aggregate. For small aggregates, the structure factor can be approximated as $S \approx 1 - q^2R_g^2/3$ (Sorensen, 2001), where $q = |\vec{q}|$ and R_g denotes the mass-averaged root-mean-square radius (radius of gyration) of an aggregate. In this regime, Eq. (2) can be rewritten as:

$$\frac{I(0)}{I(q)} \approx 1 + \frac{1}{3}q^2R_g^2 \tag{4}$$

where $I(0)$ is the intensity for forward scattering. The radius of gyration is related to the number of monomers inside an aggregate as (Mandelbrot, 1982):

$$n = \left(\frac{R_g}{r_m}\right)^{D_f} \tag{5}$$

where r_m is the monomer radius, and D_f is the aggregate's fractal dimension. By plotting $1/I(q)$ as a function of q^2, the slope and intersection with y-axis of a linear fit can provide R_g. Sorensen et al. (1995) and Sorensen (2001) have shown that $I(0)/I(q)$ versus q^2 remains linear up to $qR_g \approx \sqrt{3}$, yielding accurate values for R_g. The linear fit of a typical data set is shown in Figure 4; this flame at 1950 K and 800 ppm Si measured at HAB = 50 mm gives an R_g of ~72 nm ($qR_g < \sqrt{3}$).

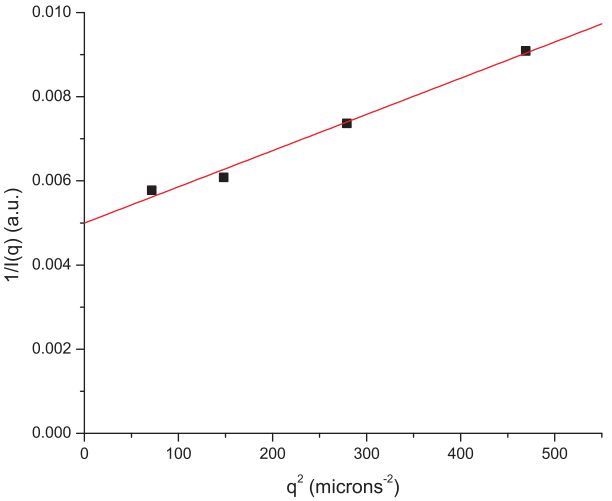

Figure 4. Linear fit of data for a 1950 K stoichiometric flame with 800 ppm silicon at HAB 50 mm giving R_g ~ 72 nm.

Results and discussion

Measurements were performed in lean (ϕ = 0.8), stoichiometric (ϕ = 1.0), and rich (ϕ = 1.3) methane/air flames at temperatures ranging from 1800 K to 2100 K and containing 300 ppm Si to 1600 ppm Si.

Dependence of aggregate size on Si concentration

The measured gyration radii R_g in stoichiometric flames at T = 1950 K are shown in Figure 5 as a function of distance above the burner for 300–1600 ppm Si in the combustion products. Stray light limited the measurement to ≥ 10 mm above the burner surface.

Part of the data was acquired outside the regime of $qR_g \leq \sqrt{3}$ for which the fitting procedure is known to yield accurate R_g (Sorensen, 2001; Sorensen et al., 1995). However, since plots of $I(0)/I(q)$ versus q^2 were found to be linear for these data, we expect the fits to still give reliable values for R_g (Sorensen, 2001).

As we can see in Figure 5, for all siloxane concentrations there is growth of aggregates with increasing HAB. At highest Si concentration of 1600 ppm, R_g increases from ~40 nm at 10 mm to ~120 nm at 50 mm. The smallest measured R_g is ~15 nm at 25 mm above the burner for 400 ppm Si. For this aggregate size, the signal difference between scattered intensities at the smallest and largest detection angle is less than 2%. Despite the fact that particles at smaller axial distances, where R_g and correspondingly the angular dependence of the scattered signal is even smaller, still generated a scattering signal a few times more intense than that in air, the fitting procedure at these heights typically yielded unreliable results. With increasing Si concentration, the minimum height where the fitting procedure could be used to yield R_g moves closer to the burner surface. We observe that extractive measurements followed by TEM analysis (Smirnov et al., 2012) for a stoichiometric flame with ~500 ppm Si at a temperature somewhat higher than here ($T \approx$ 2090 K) gives similar results to those at 500 ppm Si in Figure 5, particularly when considering the effect of temperature on R_g described below. This consistency gives additional confidence in the scattering results.

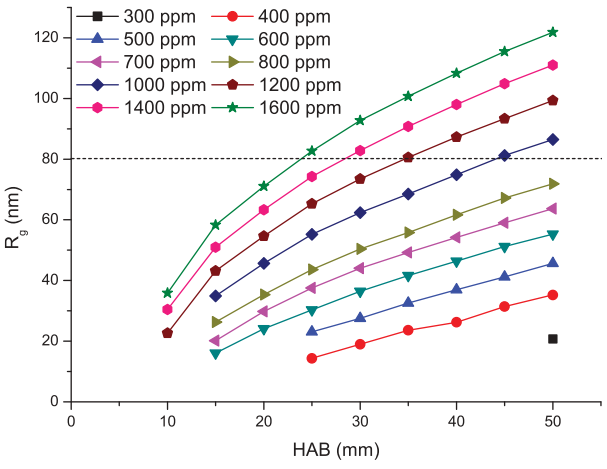

Figure 5. R_g for 1950 K stoichiometric flames as a function of axial distance above the burner, for 300–1600 ppm Si. Points above the dashed lines rely (partly) on data where $qR_g > \sqrt{3}$.

Note that the smallest aggregates measured contain very few monomers. Assuming a D_f of ~1.8 (Sorensen, 2001), an aggregate with R_g of 15 nm would contain only 3 to 18 monomers with a radius of 8 nm or 3 nm, respectively. On the other hand, an aggregate with R_g of 120 nm would contain 130 monomers of 8 nm.

For further analysis, we estimate the characteristic times of silica particle formation using simple theoretical considerations. Decomposition of siloxane proceeds in the flame front, resulting in the formation of SiO_2 molecules that condense into small clusters, which in turn collide with other molecules and clusters. For two particles containing i and j molecules, respectively, association can be schematically represented as:

$$(SiO_2)_i + (SiO_2)_j \rightarrow (SiO_2)_{i+j}$$

with a corresponding rate of $R_{i,j}$. When known, this rate can be used to find the characteristic time of association of a particle of size i with any particle of size j as $\tau_{i,j} \sim N_i/R_{i,j}$, where N_i is the concentration of particles containing i molecules. Assuming a sticking coefficient of unity, the rate of association of two particles is given by $R_{i,j} = \beta_{i,j} N_i N_j$ where $\beta_{i,j}$ is the so-called collision kernel, which depends on both particle parameters and gas properties (Friedlander, 2000). Of particular importance for determining $\beta_{i,j}$ is the ratio of the mean free path of the gas molecules λ and particle collision radius r_c, defined as the Knudsen number $Kn = \lambda/r_c$ (Kruis et al., 1993). Both for $Kn \ll 1$ and $Kn \gg 1$ (continuum and free molecular regime, respectively) theoretical expressions for the collision kernel are easily obtained (Friedlander, 2000). In a simple model where the particle is presented as a set of spheres with radius r_m (as in Eq. (5)), the collision radius, which to a good approximation is equal to the particle's radius of gyration, is related to the particle's volume v and surface area a as (Kruis et al., 1993):

$$r_c = \frac{3v}{a}\left(\frac{a^3}{36\pi v^2}\right)^{1/D_f} \tag{6}$$

For the current experimental conditions (1950 K and 1 atm) the free path length λ, calculated based on air viscosity according to Seinfeld and Pandis (2006), is approximately 550 nm. Thus, λ exceeds the measured gyration radii (Figure 5) by at least five times. It is, therefore, reasonable to use the free molecular approximation for estimation of characteristic collision times. If we assume that the particles are monodisperse, we can get a simple estimate of the time of association between two particles. In this case the collision kernel is given by (Friedlander, 2000):

$$\beta = 4r_c^2\left(\frac{\pi kT}{\rho_{SiO_2} v}\right)^{1/2} \tag{7}$$

where ρ_{SiO_2} is the density of silica and k is the Boltzmann constant; while the number density of particles N_p is given by:

$$N_p = \frac{N_{cp}\chi_{SiO_2} m_{SiO_2}}{\rho_{SiO_2} v} \tag{8}$$

where N_{cp} is the number density of the combustion products, χ_{SiO_2} is the silica mole fraction in the combustion products, and m_{SiO_2} is the molecular mass of SiO_2. Hence, for a silica concentration of 800 ppm in a 1950 K flame, the characteristic time of association of spherical particles with a 5-nm radius (thus containing ~16,000 molecules) is ~3 ms, corresponding to a height of less than 3 mm, implying that the first stage of silica formation is relatively fast and cannot be studied in the present experiment as it is well below our first measurement point at 10 mm (~12 ms). Results with TEM in a similar flame (Smirnov et al., 2012) confirmed formation of fractal structures starts very close to (within 3 mm) the burner surface.

Proceeding further with the analysis, we find the time dependence for the collision radius assuming that all silica is bound in particles and the particle density of combustion products is constant. In this case, the decay in aggregate number density N_p, due to coagulation, is given by (Friedlander, 2000):

$$\frac{dN_p}{dt} = -\frac{1}{2}\bar{\beta}N_p^2 \tag{9}$$

where $\bar{\beta}$ is the particle size averaged collision kernel. Assuming that monomer radius $r_m = 3v/a$ is constant in time, and using the assumption of a monodisperse particle size distribution and $Kn \gg 1$, we can rewrite Eq. (7) as:

$$\beta = 4\left(\frac{3}{4\pi}\right)^{\frac{2}{D_f}}\left(\frac{\pi kT}{\rho_{SiO_2}}\right)^{\frac{1}{2}} r_m^{2-\frac{6}{D_f}} v^{\frac{2}{D_f}-\frac{1}{2}} \tag{10}$$

Substituting Eqs. (8) and (10) into Eq. (9) and using relation (6) yields:

$$r_c \propto t^{2/\left(3D_f-4\right)} \tag{11}$$

The time dependence for the particle radius thus obtained is in poor agreement with the experimental results as can be seen from Figure 5. For low silica concentrations, the experimental time dependence of the particle size appears to be approximately linear, and for higher concentrations the curves clearly show a sublinear dependence, in disagreement with Eq. (11), which gives a $t^{1.43}$ dependence for $D_f \sim 1.8$. The agreement can be improved by taking D_f larger than 2, but this is at variance with available experimental observations (see, e.g., Hurd and Flower, 1988; Sneep and Ubachs, 2005; Sorensen, 2001). It is clear that this model needs to be refined.

To improve the description of particle evolution we should reconsider our assumption that the monomer size is unchanging throughout aggregate growth. This approximation essentially separates particle growth into two separate stages: monomer growth initially and the subsequent aggregation of fixed-size monomers. But this assumption ignores inter-particle monomer growth due to (partial) sintering as an important aspect of aggregate development. As is well known (Ulrich and Riehl, 1982), the growth process is actually a combination of particle collisions and simultaneous intra-aggregate fusion. This was observed in Smirnov et al. (2012), where the monomer radius was seen to increase from an initial 3 nm to 6 nm at 50 mm above the burner. Driven by a tendency to minimize surface energy, contacting monomers inside aggregates will tend to coalesce together into larger spheres, decreasing the total surface area with the rate:

$$\left(\frac{da}{dt}\right)_{\text{sintering}} = -\frac{1}{\tau_s}\left(a - a_{\text{sph}}\right) \tag{12}$$

where a is the aggregate's surface area, and τ_s is the characteristic time to reduce a to the area a_{sph} of a solid sphere of equal mass (Friedlander, 2000). If the sintering rate is fast compared to the collision rate, we expect compact sphere-like particles to be formed, while relatively slow sintering will result in aggregate-type particles. The sintering rate is a material specific property that is strongly dependent on the temperature and on the sintering mechanism. A variety of expressions have been proposed for the sintering time of silica (Goudeli et al., 2015a), but to our knowledge none are expressly applicable to the short residence times and small particle sizes relevant for the first stages of particle growth in this research. As an estimate we use an expression for bulk silica based on a viscous flow mechanism determined by Xiong et al. (1993) using data from Kingery et al. (1976), given by:

$$\tau_s = 1.3 \times 10^{-12} r_m \exp\left(\frac{8.3 \times 10^4}{T}\right) \tag{13}$$

The sintering time according to Eq. (13) at 1950 K for monomers with a radius of 5 nm is just under 20 ms. Since this is of the same order as the characteristic residence time in the present experiment (recall that HAB 10 mm corresponds to 12 ms), sintering should be taken into account in our description of particle growth, as most other formulas will give even shorter magnitudes for τ_s (Goudeli et al., 2015a). In fact, based on TEM measurements by Smirnov et al. (2012) for similar experimental conditions, we expect the monomer radius to more than double over the course of measured growth. Thus, the proper analysis of the evolution of silica particles under the present experimental conditions requires solving the system of equations describing both processes of coagulation and sintering.

Since it is not feasible to solve the equations analytically, we model the system numerically following the procedure described in Kruis et al. (1993). In these simulations, Eq. (11) is generalized by adding a term taking into account the change in gas density due to a temperature decrease downstream, and Eq. (12) is augmented with a term to account for surface growth resulting from the coagulation process. Then the system of equations becomes:

$$\frac{dv}{dt} = \left[\frac{1}{2}\beta N_p - \frac{1}{\rho_{cp}}\frac{d\rho_{cp}}{dt}\right] v \tag{14}$$

$$\frac{da}{dt} = \frac{1}{v}\frac{dv}{dt}a - \frac{1}{\tau_s}\left[a - a_{\text{sph}}\right], \tag{15}$$

where ρ_{cp} is the density of the combustion products. Because the averaged molecular mass of the combustion products remains constant, we can replace ρ_{cp} in Eq. (14) by $1/T$. In the present experiments we have observed a decrease in temperature, which for simplicity is approximated by $T(t) = T_0 \exp(-\gamma t^2)$, with $\gamma \approx 38$ s^{-2}. At 50 mm above the burner surface, the temperature had decreased from 1950 to 1700 K, resulting in a considerably increased sintering time according to Eq. (13). Furthermore, we take into account the

transition from the free molecule to continuum regime, using the semi-empirical Fuchs interpolation expression for the collision kernel (Fuchs, 1964; Seinfeld and Pandis, 2006) in which we replace the solid sphere radius by r_c:

$$\beta = 8\pi D r_c \left(\frac{r_c}{2r_c + \sqrt{2}g} + \frac{\sqrt{2}D}{c r_c} \right)^{-1} \tag{16}$$

where D is the particle diffusion coefficient, c is the mean particle velocity, and g is a transition parameter (Kruis et al., 1993). In our calculations we use a fractal dimension of 1.8, taking into consideration that the evolution of D_f from spherical to fractal-like aggregates as described by Goudeli et al. (2015b) only has a minimal impact on the results.

Starting the simulations at $t = 0$, setting the initial values of a and v to those of spheres with typical molecular radius (~0.2 nm), resulted in poor agreement with the experimental data. We attribute this primarily to the uncertainty in the estimation of the sintering time, while the model is highly sensitive to this parameter during the initial stage of aggregate growth. Using Eq. (13) for the sintering time results in gross overestimates of the rate of growth of the collision radius, because it apparently underestimates the rate of sintering for short residence times, here at $t < 10$ ms. The use of other expressions for the sintering time (Goudeli et al., 2015a) also did not reproduce the data, neither in particle size nor functional dependence on residence time. While fitting parameters in functional dependencies for sintering time such as Eq. (13) can bring agreement between the experiment and simulations, the lack of experimental data for the first stage of growth, and assumptions made in establishing the current model, dissuades us from following this procedure in the present discussion. It should be pointed out that chemistry, which was not included in the model, could also be a factor during the initial stage of growth.

To see whether the simulations can predict the functional dependence shown in Figure 5, without having to predict the initial stages in particle formation, we start the simulations at the residence time corresponding to the first point measured in each series. The initial values of $a = 4\pi r_c^{D_f} r_m^{2-D_f}$ and $v = \frac{4}{3}\pi r_c^{D_f} r_m^{3-D_f}$ are set by using the measured value of R_g as the collision radius r_c and adjusting the monomer radius r_m. Furthermore, a scaling factor c was included in expression (13) for the sintering time $\tau = c\tau_s$. The best agreement between the experimental and calculated r_c for all silica concentrations is achieved with the scaling factor $c \gtrsim 10$, essentially disabling particle coalescence though sintering at times after initial particle formation. The analysis in Wooldridge et al. (2002) resulted in a similar conclusion. The results of simulations for 400, 800, and 1600 ppm of silica with the values for r_m obtained by fitting of 5.5 nm, 4.3 nm, and 3 nm, respectively, are shown in Figure 6, where residence times for experimental data were calculated using the measured flow rates and estimated flame temperatures. We see that the experimental data for higher silica concentrations require a smaller value of r_m, while it is expected that the additional available silica would result in larger monomers. At the same time, we point out that even without sintering the model accounts perfectly well for the sublinear time dependence of r_c; this is the result of using Fuchs' interpolation expression for the collision kernel rather than the free molecular assumption that was used to get Eq. (11). We report that the simulated results were relatively insensitive to the temperature history

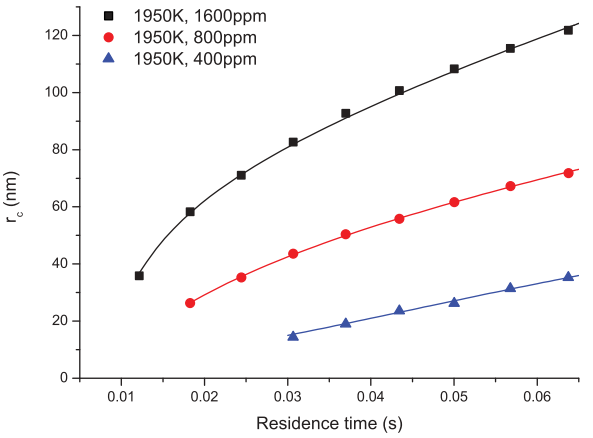

Figure 6. Numerical simulations for silica concentrations of 400, 800, and 1600 ppm obtained by matching the collision radius with the initial data point of each series.

used as a result of the temperature dependence of Eq. (13) and were more sensitive to the initial particle size. This emphasizes the need for more experimental information on the initial stages of particle growth.

Temperature dependence

The measured gyration radii R_g in stoichiometric flames at temperatures ranging from 1800 K to 2100 K for a fixed concentration of 800 ppm silica in the combustion products are shown in Figure 7 as a function of residence time.

These experimental data show a non-monotonic dependence of aggregate growth on the flame temperature. When the flame temperature increases from 1800 K to 2000 K, R_g corresponding to a given residence time increases as well, whereas in the temperature

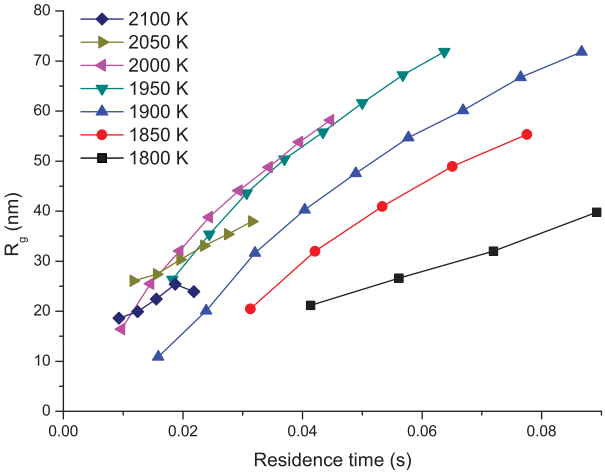

Figure 7. R_g for stoichiometric flames as a function of residence time with different temperatures; 800 ppm Si in the gases.

range above 2000 K we observe either constant or a slight decrease in R_g at the same residence time with increasing temperature. The smaller R_g for the highest temperatures, which are above the melting point of bulk silica (Lide, 2003), are attributed to fast sintering, resulting in relatively compact particles consisting of large monomers. Interestingly, the opposite does not hold true for temperatures below 2000 K, where, in the framework of the model, we would expect the low sintering rates to result in relatively fast formation of large, low-density structures, while the impact of the change in temperature on the collision kinetics is marginal. Given the changes in temperature close to the bulk melting point, the possibility of increased clustering of monomers caused by progressively enhanced viscous attachment as the temperature is raised from 1800 K to 1950 K could stabilize larger clusters more easily than association by van der Waals attraction (Goudeli et al., 2015b). However, at the relatively short time scales of the experiment the sintering rates to coalescence, resulting in denser clusters, are still relatively slow below 2000 K. Another effect, intrinsic to laminar, burner-stabilized flames is possible thermophoretic transport of very small silica clusters upstream from the flame front, even to the burner surface, which can increase when decreasing the mass flux. Although it is unlikely that substantial fractions of the silica particles will be deposited at the burner by this mechanism, additional experiments and detailed modeling will be required to describe this process adequately.

We also note that many practical combustion equipment operates with such variations in temperature at the residence times, are reported here. Thus, the large variation in particle size when changing operating conditions can impact the rates of silica deposition in practical equipment; this also suggests that operating regimes may exist for equipment intended to minimize the effects of deposition, which will be investigated in the future.

Using the numerical simulations, we could achieve a fit of comparable agreement as seen in Figure 6, when varying the monomer radius r_m. For temperatures of 1850 K, 1950 K, and 2050 K, the "best fit" monomer radii, r_m, are 6.2 nm, 4.3 nm, and 5.8 nm, respectively, which reflect the non-monotonic dependence of r_c. The larger r_m for 2050 K compared to 1950 K corresponds with the expectation of more compact particles, but the suggestion indicated by Zachariah et al. (1989b), that changes in nucleation lead to larger particles at relatively low temperatures, seems at present the only explanation for the larger r_m for 1850 K. Other experiments, in which the monomer radius is measured at low Si concentration and short residence times, are required to better explain the observed influence of temperature on particle growth.

Dependence of aggregate growth on equivalence ratio

As mentioned in the introduction, most of the experiments on premixed flames have varied the flame temperature together with the equivalence ratio. Here, we maintain the flame temperature by changing the mass flux through the burner. Aggregate growth was studied in lean (ϕ = 0.8), stoichiometric and rich (ϕ = 1.3) flames at 1850 K and 1950 K, doped with 800 ppm Si. The results, presented in Figures 8 and 9, respectively, show a remarkable difference between particle growth in a lean flame environment on the one hand, and stoichiometric and rich environments on the other. The oxygen-rich environment appears to greatly stimulate aggregate growth, up to a factor of 2 as compared to the other equivalence ratios, while there is no significant difference between particle growth in

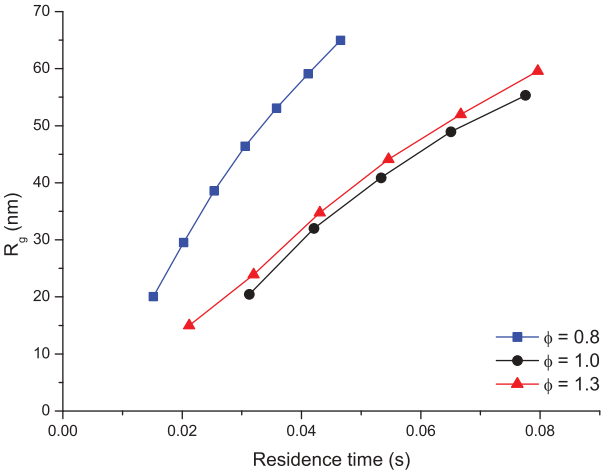

Figure 8. R_g versus residence time at 1850 K for three equivalence ratios; doping of 800 ppm Si.

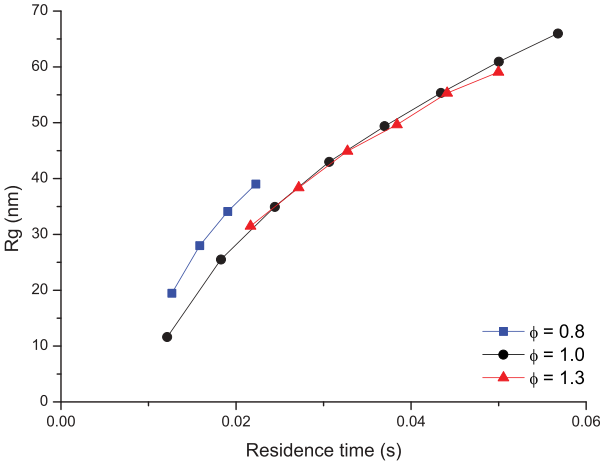

Figure 9. R_g versus residence time at 1950 K for three equivalence ratios; doping of 800 ppm Si.

stoichiometric and fuel-rich (oxygen-poor) flames. Comparison with stoichiometric flames of higher temperatures (e.g., as in Figure 7) shows that the observed difference is well in excess of what might reasonably be attributed to a slight variation in flame temperature due to the small uncertainty in conditions.

The model described above, because there is little difference in transport properties between the combustion products at different equivalence ratios, will not reflect a dependence on equivalence ratio. There are very few published studies that examine particle growth with a comparable variation in parameters. In Butler et al. (2002), particle formation was also considered in a very rich premixed ($\varphi = 3$) H_2/O_2 flame doped with L2, where they raised the possibility of other silicon-containing species such as SiO condensing with the particles. Although simple equilibrium calculations indicate that silica should be the major condensed species, even at $\varphi = 1.3$, it is premature to exclude kinetic effects in silica formation for the temperatures and residence times presented here. Conditions of excess oxygen in which we

expect SiO_2 to be the only condensing species appear to foster particle aggregation, particularly at lower temperatures where we expect sintering to be relatively slow, as described above. For conditions of low oxygen, a mechanism by which SiO or other species (Butler et al., 2002) deposits with silica in the primary particles either inhibits aggregate growth, particularly at lower temperatures, or (strongly) enhances sintering to generate denser particles. Measurement of primary particle size is necessary to discriminate between these mechanisms.

Summary and conclusions

ADLS measurements in 1D premixed methane/hexamethyldisiloxane/air flames showed a sublinear dependence of the radii of gyration R_g of generated silica particles on residence time, and a non-monotonic dependence on flame temperature with a maximum around 2000 K. Interestingly, a lean flame environment appears to foster aggregate growth compared to rich and stoichiometric flames in which growth is very similar. This result implies an unexpected dependence of aggregate formation on oxygen fraction and warrants further research, both to explore regimes for influencing particle growth (Ulrich and Riehl, 1982) and to assess the impact of silica formation and deposition in practical combustion equipment (Gersen et al., 2013; Turkin et al., 2014). The results presented here recommend caution when altering the equivalence ratio as a means to study the effect of flame temperature on particle growth.

Using a simple model to describe particle evolution from $t = 0$ as a result of collisional growth and sintering was frustrated by the lack of an accurate expression for the sintering time, for the time scales and particle sizes in the experiment, and an incomplete understanding of the first stages of particle growth where chemistry may still be relevant. Using initial conditions derived from the experimental data, at times greater than ~10 ms, the model describes aggregate growth adequately but suffers from the necessity of fitting the monomer radius. It is crucial to acquire more data for the initial stage of growth to explain the observed dependence of R_g on temperature and equivalence ratio. We plan to perform TEM measurements in the future to augment the ADLS-acquired experimental data, particularly to characterize the development of monomer size. This would also allow for determination of D_f and the average number of monomers in fractal aggregates for the flame conditions considered here.

Funding

This research has been financed by a grant from the Energy Delta Gas Research (EDGaR) program. EDGaR is co-financed by the Northern Netherlands Provinces, the European Fund for Regional Development, the Ministry of Economic Affairs, Agriculture and Innovation, and the Province of Groningen.

References

Bae, S.H., and Shin, H.D. 2009. Generation of silica nanoparticles in turbulent non-premixed flames with oxygen enrichment. *Energy Fuels*, **23**, 5338–5348.

Butler, C.J., Hayhurst, A.N., and Wynn, E.J.W. 2002. The size and shape of silica particles produced in flames of $H_2/O_2/N_2$ with a silicon-containing additive. *Proc. Combust. Inst.*, **29**, 1047–1054.

Chang, H., Chang, H., Hong, H., and Won, Y. 1998. Optical characterization of the nonspherical aerosol particles generated by combustion. *Environ. Eng. Res.*, **3**, 79–86.

Choi, M., Cho, J., Lee, J., and Kim, H.W. 1999. Measurements of silica aggregate particle growth using light scattering and thermophoretic sampling in a coflow diffusion flame. *J. Nanopart. Res.*, **1**, 169–183.

Flaningam, O.L. 1986. Vapor pressures of poly(dimethylsiloxane) oligomers. *J. Chem. Eng. Data*, **31**, 266–272.

Flower, W.L., and Hurd, A.J. 1987. In situ measurement of flame-formed silica particles using dynamic light scattering. *Appl. Opt.*, **26**, 2236–2239.

Friedlander, S.K. 2000. *Smoke, Dust and Haze: Fundamentals of Aerosol Dynamics*, Second ed., Oxford University Press, New York.

Fuchs, N.A., 1964. *The Mechanics of Aerosols*, Pergamon Press, Oxford.

Gersen, S., Visser, P., van Essen, V.M., Dutka, M., Vainchtein, D., de Hosson, J.T.M., and Levinsky, H.B. 2013. Effects of silica deposition on the performance of domestic equipment. In *Proceedings of the European Combustion Meeting*, Lund, Sweden, June 25–28, pp. P1–51.

Goodwin, D.G., Moffat, H.K., and Speth, R.L. 2015. *Cantera: An Object-Oriented Software Toolkit for Chemical Kinetics, Thermodynamics, and Transport Processes*. Version 2.20. http://www.cantera.org.

Goudeli, E., Eggersdorfer, M.L., and Pratsinis, S.E. 2015a. Aggregate characteristics accounting for the evolving fractal-like structure during coagulation and sintering. *J. Aerosol Sci.*, **89**, 58–68.

Goudeli, E., Eggersdorfer, M.L., and Pratsinis, S.E. 2015b. Coagulation–agglomeration of fractal-like particles: Structure and self-preserving size distribution. *Langmuir*, **31**, 1320–1327.

Hurd, A.J., and Flower, W.L. 1988. In situ growth and structure of fractal silica aggregates in a flame. *J. Colloid Interface Sci.*, **122**, 178–192.

Jalali, A., Motamedhashemi, M.M.Y., Egolfopoulos, F., and Tsotsis, T. 2013. Fate of siloxane impurities during the combustion of renewable natural gas. *Combust. Sci. Technol.*, **185**, 953–974.

Jang, H.D. 1999. Generation of silica nanoparticles from tetraethylorthosilicate (TEOS) vapor in a diffusion flame. *Aerosol Sci. Technol.*, **30**, 477–488.

Kingery, W.D., Bowen, H.K., and Uhlmann, D.R. 1976. *Introduction to Ceramics*, Wiley, New York.

Kruis, F.E., Kusters, K.A., Pratsinis, S.E., and Scarlett, B. 1993. A simple model for the evolution of the characteristics of aggregate particles undergoing coagulation and sintering. *Aerosol Sci. Technol.*, **19**, 514–526.

Lee, B.W., Jeong, J.I., Hwang, J.Y., Choi, M., and Chung, S.H., 2001a. Analysis of growth of non-spherical silica particles in a counterflow diffusion flame considering chemical reactions, coagulation and coalescence. *J. Aerosol Sci.*, **32**, 165–185.

Lee, B.W., Oh, S., and Choi, M. 2001b. Simulation of growth of nonspherical silica nanoparticles in a premixed flat flame. *Aerosol Sci. Technol.*, **35**, 978–989.

Lide, D.R. (Ed.). 2003. *Handbook of Chemistry and Physics*, 84th ed., CRC Press, London.

Mandelbrot, B.B. 1982. *The Fractal Geometry of Nature*, W.H. Freeman and Co., New York.

Mokhov, A.V., and Levinsky, H.B. 2000. A LIF and CARS investigation of upstream heat loss and flue-gas recirculation as NOx control strategies for laminar, premixed natural-gas/air flames. *Proc. Combust. Inst.*, **28**, 2467–2474.

Mokhov, A.V., Smirnov, B.M., and Dutka, M. 2013. Formation of chain aggregates in external electric field. *Chem. Phys.*, **570**, 104–108.

Pratsinis, S.E. 1998. Flame aerosol synthesis of ceramic powders. *Prog. Energy Combust. Sci.*, **24**, 197–219.

Rasi, S. 2009. *Biogas Composition and Upgrading to Biomethane*, University of Jyväskylä, Jyväskylä, Finland.

Rulison, A.J., Miquel, P.F., and Katz, J.L. 2011. Titania and silica powders produced in a counter-flow diffusion flame, *J. Mater. Res.*, **11**, 3083–3089.

Seinfeld, J.H., and Pandis, S.N. 2006. *Atmospheric Chemistry and Physics: From Air Pollution to Climate Change*, 2nd ed., John Wiley & Sons, Inc., Hoboken, NJ.

Sepman, A.V., Mokhov, A.V., and Levinsky, H.B. 2011. Extending the predictions of chemical mechanisms for hydrogen combustion: Comparison of predicted and measured flame temperatures in burner-stabilized, 1-D flames, *Int. J. Hydrogen Energy*, **36**, 9298–9303.

Sepman, A.V., Toro, V.V., Mokhov, A.V., and Levinsky, H.B. 2013. Determination of temperature and concentrations of main components in flames by fitting measured Raman spectra, *Appl. Phys. B*, **112**, 35–47.

Shekar, S., Sander, M., Riehl, R.C., Smith, A.J., Braumann, A., and Kraft, M. 2012. Modelling the flame synthesis of silica nanoparticles from tetraethoxysilane. *Chem. Eng. Sci.*, **70**, 54–66.

Smirnov, B.M. 2011. Processes involving clusters and small particles in a buffer gas. *Phys. Usp.*, **54**, 691–721.

Smirnov, B.M., Dutka, M., van Essen, V.M., Gersen, S., Visser, P., Vainchtein, D., de Hosson, J.T. M., Levinsky, H.B., and Mokhov, A.V. 2012. Growth of fractal structures in flames with silicon admixture. *Europhys. Lett.*, **98**, 66005.

Smith, G.P., Golden, D.M., Frenklach, M., Moriarty, N.W., Eiteneer, B., Goldenberg, M., Bowman, C.T., Hanson, R.K., Song, S., Gardiner, W.C., Lissanski, J.V.V., Qin, Z., n.d. GRI-MECH 3.0 [WWW Document]. Available at: http://www.me.berkeley.edu/gri_mech/.

Sneep, M., and Ubachs, W. 2005. Direct measurement of the Rayleigh scattering cross section in various gases. *J. Quant. Spectrosc. Radiat. Transfer*, **92**, 293–310.

Sorensen, C.M. 2001. Light scattering by fractal aggregates: A review. *Aerosol Sci. Technol.*, **35**, 648–687.

Sorensen, C.M., Lu, N., and Cai, J. 1995. Fractal cluster size distribution measurement using static light scattering. *J. Colloid Interface Sci.*, **174**, 456–460.

Suh, J.S., Kim, C.S., Kim, T.O., and Choi, M. 2006. Structural and chemical characterization of SiO_2/TiO_2 multicomponent particles during aerosol formation in a coflow diffusion flame. *Adv. Powder Technol.*, **17**, 495–508.

Suh, S.-M., Zachariah, M.R., and Girshick, S.L. 2001. Modeling particle formation during low-pressure silane oxidation: Detailed chemical kinetics and aerosol dynamics. *J. Vac. Sci. Technol*, **19**, 940.

Turkin, A.A., Dutka, M., Vainchtein, D., Gersen, S., Essen, V.M. van, Visser, P., Mokhov, A.V., Levinsky, H.B., and de Hosson, J.T.M. 2014. Deposition of SiO_2 nanoparticles in heat exchanger during combustion of biogas. *Appl. Energy*, **113**, 1141–1148.

Ulrich, G.D., and Riehl, J.W. 1982. Aggregation and growth of submicron oxide particles in flames. *J. Colloid Interface Sci.*, **87**, 257–265.

van Foreest, F. 2012. *Perspectives for Biogas*, Oxford.

Wooldridge, M.S. 1998. Gas-phase combustion synthesis of particles. *Prog. Energy Combust. Sci.*, **24**, 63–87.

Wooldridge, M.S., Torek, P.V., Donovan, M.T., Hall, D.L., Miller, T.A., Palmer, T.R., and Schrock, C.R. 2002. An experimental investigation of gas-phase combustion synthesis of SiO_2 nanoparticles using a multi-element diffusion flame burner. *Combust. Flame*, **131**, 98–109.

Xiong, Y., Kamal Akhtar, M., and Pratsinis, S.E. 1993. Formation of agglomerate particles by coagulation and sintering—Part II. The evolution of the morphology of aerosol-made titania, silica and silica-doped titania powders. *J. Aerosol Sci.*, **24**, 301–313.

Zachariah, M.R., Chin, D., Semerjian, H.G., and Katz, J.L. 1989a. Dynamic light scattering and angular dissymmetry for the in situ measurement of silicon dioxide particle synthesis in flames. *Appl. Opt.*, **28**, 530.

Zachariah, M.R., Chin, D., Semerjian, H.G., and Katz, J.L. 1989b. Silica particle synthesis in a counterflow diffusion flame reactor. *Combust. Flame*, **78**, 287–298.

Zachariah, M.R., and Semerjian, H.G. 1989. Simulation of ceramic particle formation: Comparison with in-situ measurements. *AIChE J.*, **35**, 2003–2012.

Zhu, W., and Pratsinis, S.E. 1997. Synthesis of SiO_2 and SnO_2 particles in diffusion flame reactors. *AIChE J.*, **43**, 2657–2664.